ChemBioChem

Research Article
doi.org/10.1002/cbic.202400143

**Chemistry
Europe**
European Chemical
Societies Publishing

www.chembiochem.org

Reversible Influence of Hemipiperazine Photochromism on the Early Development of Zebrafish Embryo

Angelika Seliwjorstow+,[a] Masanari Takamiya+,[b] Sepand Rastegar,*[b] and
Zbigniew Pianowski*[a, c]

This study explores the potential of controlling organismal development with light by using reversible photomodulation of activity in bioactive compounds. Specifically, our research focuses on plinabulin **1**, an inhibitor of tubulin dynamics that contains a photochromic motif called hemipiperazine. The two isomeric forms, Z-**1** and E-**1**, can partially interconvert with light, yet show remarkable thermal stability in darkness. The Z-isomer exhibits higher cytotoxicity due to stronger binding to α-tubulin's colchicine site. The less toxic E-**1** form, considered a "pro-drug", can be isolated *in vitro* and stored. Upon activation by blue or cyan light, it predominantly generates the more toxic Z-**1** form. Here we demonstrate that **1** can effectively photo-modulate epiboly, a critical microtubule-dependent cell movement during gastrulation in zebrafish embryos. This research highlights the potential of photomodulation for precise and reversible control of cellular activities and organismal development.

Introduction

Living organisms' interactions with light rely on light-sensitive proteins, such as rhodopsin, light-oxygen-voltage proteins, cryptochromes, and phytochromes, which encompass chromophores capable of altering their structure upon photon absorption. This phenomenon leads to modifications in their activity, or the resultant change is transmitted to an effector. Utilizing genetic engineering, light has been harnessed to both observe and regulate a myriad of cellular activities, leading to the emergence of the field known as "optogenetics"[1] . An alternative strategy involves conferring photosensitivity upon bioactive small molecules.[2] This is frequently achieved by introducing or substituting specific components of their structure with molecular photoswitches[3] - substances that exhibit reversible alterations in properties (such as shape and polarity) upon exposure to light, with azobenzene derivatives[4] being the most commonly used. This emerging approach known as "photopharmacology"[5] has given rise to a plethora of compounds with potential antimicrobial[6] and anticancer applications.[7] Examples include photoactivated antibiotics,[8] estrogen receptor antagonists,[9] inhibitors of serine proteases,[10] dihydrofolate reductase (DHFR),[11] histone deacetylase (HDAC),[12] actin dynamics,[13] and microtubule dynamics.[14] A notably captivating category encompasses inhibitors of tubulin polymerization that specifically target the colchicine binding site.[15] This endeavor involves the structural adaptation of the naturally occurring stilbenoid combretastatin A4, which yielded azobenzene-based photostatins[16] and a series of optimized derivatives based on various photochromic motifs.[7,17] Our group discovered[18] that another tubulin dynamics inhibitor, plinabulin **1**, contains a previously unreported photochromic motif – hemipiperazine[19] – which enables significant photomodulation of the activity of **1** without additional structural modifications.

Given the significance of cytoskeleton dynamics in cellular functions, the introduction of photoswitchable inhibitors represents an innovative avenue for finely tuned control over organismal development in both spatial and temporal dimensions. Photostatins, for instance, have been successfully employed to regulate epithelial morphogenesis in *D. melanogaster*[20] as well as intracellular transport during the early stages of mouse embryogenesis.[21] Furthermore, a styrylbenzothiazole combretastatin analogue has enabled the manipulation of microtubule dynamics *in vivo* across a diverse array of models, including organoids, zebrafish, clawed frogs, and the fly brain.[22]

Plinabulin **1** is an investigational anticancer drug being studied in multiple FDA clinical trials, both as a standalone treatment and in combination with other drugs. These trials

[a]   A. Seliwjorstow,+ Dr. Z. Pianowski
      Institute of Organic Chemistry,

      Karlsruhe Institute of Technology KIT;
      Kaiserstrasse 12, 76131 Karlsruhe, Germany
      E-mail: pianowski@kit.edu

[b] Dr. M. Takamiya,+ Dr. S. Rastegar
      Institute of Biological and Chemical Systems – Biological Information Processing IBCS-BIP,
      Karlsruhe Institute of Technology KIT;
      Kaiserstrasse 12, 76131 Karlsruhe, Germany
      E-mail: sepand.rastegar@kit.edu

[c] Dr. Z. Pianowski
      Institute of Biological and Chemical Systems – Functional Molecular Systems IBCS-FMS,
      Karlsruhe Institute of Technology KIT;
      Kaiserstrasse 12, 76131 Karlsruhe, Germany

[+] Joint first authors.

ChemBioChem

Research Article
doi.org/10.1002/cbic.202400143

Chemistry Europe
European Chemical
Societies Publishing

target conditions such as non-small cell lung cancer (NCT02504489),[23] other tumors,[24] and TAC-induced neutropenia.[25] The intriguing potential to modulate its effects using light, particularly within living organisms, opens up exciting possibilities for utilizing plinabulin in photopharmacological applications and advancing the development of highly selective and spatiotemporally precise antitumor phototherapies. **1** can exist in two isomeric forms: Z-**1** and E-**1**,[18] which reversibly interconvert upon exposure to light in the range of 365–490 nm. In the absence of light, Z-**1** is indefinitely stable, while the E-**1** form remains metastable at room temperature, gradually converting to the Z-form with the half-life of >1 month. In the experiments conducted within the specified timeframe (<48 h) and under the defined conditions, the amount of thermally generated Z-**1** remains negligible. As previously demonstrated[18], the isomers can be isolated in pure forms (>95% each) using HPLC chromatography. They exhibit significant differences in cytotoxicity against mammalian cells, as determined by cell viability assays (MTT) performed on the human cancer HT-29 cell line. The Z-isomer exhibits stronger binding to the colchicine binding site of α-tubulin compared to the geometrically distorted E-isomer, which explains the observed cytotoxicity difference. In our recent work, we have also demonstrated through immunostaining that **1** affects the cytoskeleton assembly in these cells in a light-dependent manner.[18] The less toxic E-**1** isomer can be isolated and stored for months in the freezer without significant back-isomerization. Thus, it can be considered a "pro-drug"-like compound. It can be further activated using blue or cyan light (450–490 nm) at the desired time and location. Upon activation, E-**1** generates a mixture predominantly (up to 87%) composed of the more toxic Z-**1**. The most significant cytotoxicity photomodulation (85-fold increase) is achieved in this irreversible "photouncaging without cage" mode of use, while reversible switching between mixtures photoequilibrated with cyan light (490 nm) and UV light (365 nm) results in an approximately 40-fold difference in activity.[18]

In this study, our goal was to examine and characterize the effects of plinabulin, specifically its responsiveness to photomodulation, within an *in vivo* model-zebrafish embryos. Zebrafish serves as an immensely valuable animal model,[26] offering numerous advantages in exploring the photomodulation of **1** within an organismal context. Its reliability as a model organism allows for the translation of initial *in vitro* cytotoxicity data into a realistic setting, encompassing considerations of pharmacokinetics, dynamics, and potential side effects beyond the fundamental mode of action.[27] The zebrafish's transparency is particularly advantageous, facilitating optical imaging of molecular, cellular, and systemic effects induced by **1**. This aspect is further enhanced by the availability of various transgenic lines featuring fluorescence markers that target nuclear structures or tubulin — the primary target of plinabulin. Moreover, the rapid developmental pace of zebrafish embryos offers a valuable window to investigate critical biological processes during early development, including epiboly and nervous system formation.[28]

We specifically focus on monitoring the epiboly process, occurring between 4 hpf (hours post-fertilization) and 10 hpf. Epiboly is a microtubule-dependent[29] cell movement integral to gastrulation in zebrafish embryos.[30] It involves coordinated thinning and spreading movements of the blastoderm (cellular part of the embryo excluding the yolk cell) and the yolk syncytial layer (YSL). YSL is an unique organ to teleost fish which is formed at the margin of the blastoderm facing to the yolk cell.[31] Although YSL itself does not contribute to the body of the embryo, it is essential for normal embryonic development through its involvement in patterning, morphogenesis and metabolism.[32] Additionally, our objective involves evaluating the impact of drug's activity photomodulation on the embryo's normal development, achieved by observing the phenotype of treated embryos at 24 and 48 hpf.

We demonstrate that the modulation of activity of **1** with light has a meaningful influence on the epiboly process, and it can be used to influence the early stages of zebrafish embryo development in a predictable and concentration-dependent manner (Figure 1).
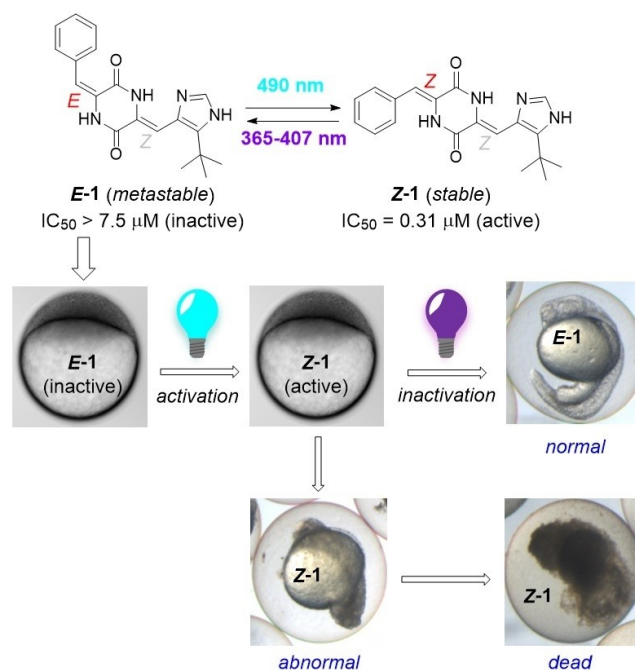

Figure 1. The Effect of Plinabulin Photoisomerization on Zebrafish Embryos. Plinabulin **1** inhibits microtubule dynamics, and can be photoisomerized between two thermally (meta)stable isomers with different activities. Here, we use **1** to reversibly control the epiboly in zebrafish embryos. The mitotic arrest caused by accumulation of the more toxic Z-**1** can be reversed with light, before irreversible apoptosis takes place leading to embryos' death.

ChemBioChem

Research Article
doi.org/10.1002/cbic.202400143

**Chemistry
Europe**
European Chemical
Societies Publishing

Results

Plinabulin Spontaneously Penetrates Zebrafish Embryos and Exhibits Isomer-dependent Toxicity

We conducted an assessment of capacity of compound **1** to penetrate zebrafish embryos, concurrently establishing its toxicity spectrum during the initial stages of zebrafish development. Specifically, fertilized eggs (20 eggs per vial) were subjected to treatment at 4 hpf with ascending concentrations of **1**. This encompassed the administration of the purified *Z*-isomer (highly toxic), the purified *E*-isomer (displaying lower toxicity), as well as a photoequilibrated mixture (designated as 69% *Z*-**1**, as shown in **Table S1**) that was obtained by irradiation of the purified *E*-**1** with cyan light (490 nm) upon 60 min.

The substance exhibits efficient absorption from the fish water into the embryos and triggers a toxic effect comparable to that observed in previous cell culture experiments.[18] The toxicity of each treatment, characterized by its concentration dependence, is illustrated in **Figure S5**. The LD_{50} values we determined are as follows: 0.31 μM for *Z*-**1**, > 7.5 μM for *E*-**1**, and > 1 μM for the photoequilibrated mixture containing 69% of *Z*-**1**. To reinforce the validity of these findings, we have verified them through the phenotypic alterations observed after 24 hpf in embryos treated with sub-lethal concentrations of compound **1**, as depicted in Figure 2 and **Figure S6**.

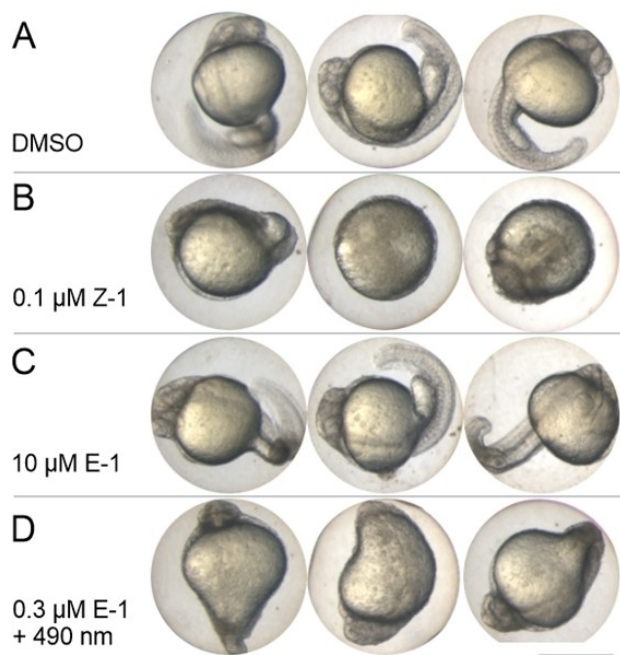**Figure 2. Phenotypic Effects of Different Isomeric Compositions of Plinabulin on Zebrafish Embryos for Sublethal Concentrations. A)** negative control (DMSO 0.125%) – No abnormal phenotype observed. **B)** 0.1 μM *Z*-**1** ($LD_{50}=0.31$ μM) – Severe malformation evident in embryos. **C)** 10 μM *E*-**1** ($LD_{50}>7.5$ μM) – Embryos exhibit normal appearance with no malformations or deaths. **D)** 0.3 μM *E*-**1** irradiated with cyan light (490 nm) ($LD_{50}>1$ μM for that mixture) – Embryos display malformation. Three representative embryos are depicted for each scenario. All pictures taken at 24 hpf. Scale bar: 500 μm.

Cellular Mechanisms of Plinabulin Toxicity and Malformations of Zebrafish Embryos

Subsequently, we delved into the cellular-level mechanisms underlying the observed overall toxicity and abnormal embryonic development depicted in Figure 2. To achieve this, we analyzed embryos at an earlier developmental stage during gastrulation after the treatment with or without *Z*-**1** starting at 2.5 hpf. After fixing the treated embryos at 6 hpf, we acquired images in bright field view, DAPI nucleus staining and alpha-tubulin immunostaining (Figure 3). In the bright field view, the embryos treated with Z-1 (3 μM) exhibited thicker blastoderm (Figure 3E) than DMSO control (Figure 3A), suggesting defects in epiboly progression. Nucleus staining showed less densely packed nuclei with a substantial space in-between in the blastoderm (nuclei located animal to the blastoderm margin [region above the magenta line]) and abnormal YSL nucleus position that is closer to the blastoderm margin (nuclei located vegetal to the margin; arrows) for the Z-1 treated embryos (Figure 3F). Tubulin immunostaining showed abnormal accumulation in the blastomere cells (cells located animal to the margin) and YSL (Figure 3G–H), suggesting Z-1 affects microtubule dynamics of both structures.

Abnormal and Incomplete Epiboly upon Photomodulation of E-1 into Z-1 in Vivo

Decreased nucleus number in the blastoderm and YSL after *Z*-1 treatment can be caused by various reasons such as cell death and inhibition of cell division. In order to understand how this phenotype is caused by Z-1, we employed a zebrafish trans-
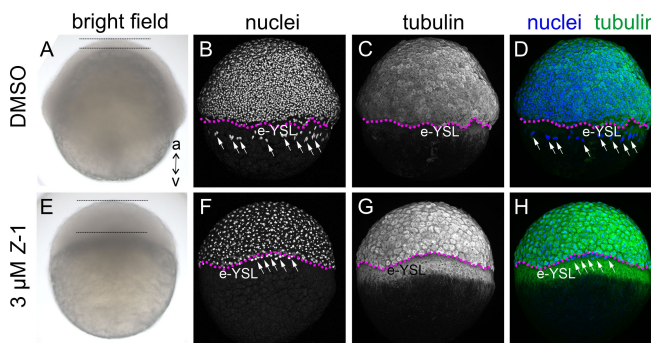

Figure 3. Treatment of Embryos with *Z*-1 Arrests Cell Division and Epiboly Movements. Phenotypic comparison between control (**A-D**, DMSO) and embryos treated with *Z*-**1** (3 μM) (**E-H**) at 6 hpf, showcased through: (**A** and **E**) bright field view, (**B** and **F**; grayscale) DAPI nuclei staining, (**C** and **G**; grayscale) tubulin immunohisto staining, (**D** and **H**; nuclei in blue and tubulin in green) merged view of nuclei and tubulin; The animal pole (a) is oriented upwards, while the vegetal pole (v) is directed downwards. Notably, the *Z*-1-treated embryo (**E**) displays thickening of the blastoderm (span between two horizontal bars), a contrast to the control (**A**). Anomalous accumulation of tubulin is observed in the yolk syncytial layer (YSL) of *Z*-1-treated embryos, forming a belt-like structure vegetal to the blastoderm margin (stippled magenta line). The YSL nuclei (white arrows) were confined at the close vicinity of the blastoderm margin in the Z-1 treated embryo (**F**), while in the control they were found away from the margin and more in the vegetal region (**B**). Scale bar: 100 μm.

ChemBioChem

Research Article
doi.org/10.1002/cbic.202400143

Chemistry Europe
European Chemical
Societies Publishing

genic line tagged with fluorescently labeled nuclei (Tg(actb2: H2 A-mCherry)) and illuminated with blue light to modulate the bioactivity of E-**1** in living embryos. In our assessment, we examined a sample treated with 1 μM E-**1** (the less toxic isomer) in the absence of light, and compared it with the sample prepared under the same conditions and subjected to blue light irradiation for 3 minutes (450–490 nm light from a mercury lamp source with the I3 filter using a DMi8 inverted microscope STED/SP8; Leica Microsystems, Wetzlar) to generate the more toxic Z-**1** isomer in situ. Furthermore, to estimate the isomeric composition in the latter experiment, we have irradiated a more concentrated (1 mM, due to limited detection sensitivity) solution of E-**1** with the aforementioned light source for a duration of 3 minutes, where subsequent HPLC analysis disclosed the presence of 67% Z-**1** (**Table S2**). The ensuing step involved the visualization of cell nucleus dynamics and proliferation in living embryos. In **Movie S1**, spanning the interval from 4.5 hpf to 20 hpf, the antiproliferative impact of light-activated plinabulin (as the Z-isomer) becomes evident, along with the inhibition of proper development and eventual embryo death around 15 hpf. The crucial time points are delineated in Figure 4. At 30%-epiboly stage (Figure 4A, **F**), the E-**1**-treated embryos showed similar number and distribution pattern of external yolk syncytial nuclei (e-YSN; white arrows) in the region directly vegetal to the blastoderm margin with or without blue light illumination.

However, toward the development to 75%-epiboly stage, e-YSN of blue light-illuminated group showed abnormal coordinated animal-ward migration (Figure 4B–C, G–H; **Movie S1**), often forming clusters (arrowheads), and finally migrated completely beneath the blastomere at bud stage (Figure 4D, I). As a result, the epiboly of blue light-illuminated embryos remained still incomplete (Figure 4J) with the vegetal-most yolk uncovered by the blastoderm, when non-blue light-illuminated group started to form the tail structure (Figure 4E). Thus, the non-toxic E-**1** can be efficiently converted into the toxic Z-**1** in vivo. We also identified the abnormal animal-ward movement of yolk syncytial nuclei as a cause of their decreased number.

Figure 4. Real-time Imaging of Embryo Development Using a Fluorescently Labeled Nuclei Transgenic Line (magenta; Tg(actb2:H2 A-mCherry)). The upper row of each panel shows an embryo treated with 1 μM of E-**1** without exposure to the blue light (450-490 nm) (**A**-**E**), and the lower panels show an embryo treated with the same reagent and further exposed to the blue light to produce the Z-**1** isomer in situ (**F**–**J**). Stages are 30% epiboly (4.7 hpf; **A**, **F**), 60% epiboly (6.8 hpf; **B**, **G**), 75% epiboly (7.9 hpf; **C**, **H**), bud stage (9.6 hpf; **D**, **I**) and 14 somite stage (16 hpf; **E**, **J**). The stippled white line demarcates the blastoderm margin. The external yolk syncytial nuclei (e-YSN) are pointed by arrows. Note that the e-YSN normally migrate toward the vegetal pole in the control (**A**-**C**). After blue light illumination, however, a group of e-YSN (**F**–**H**, arrowhead) together with other e-YSNs (arrows) abnormally migrates toward the animal pole relative to the blastoderm margin (stippled white line) and becomes internalized beneath the blastoderm. As a result, the epiboly was arrested at later stages (**I**–**J**). For early stages (**A**-**C** and **F**–**H**) the embryo is oriented the animal (a) pole up and the vegetal (v) pole down. Scale bar: 100 μm; (**K**–**P**) Schematics of the E-**1** treated gastrulae highlighting the external yolk syncytial layer (e-YSL brown) at stages of 50% epiboly (**K**, **N**), 75% epiboly (**L**, **O**) and 90% epiboly (**M**, **P**), with (**N**-**P**) or without (**K**-**M**) blue light illumination. Note the abnormal animal-ward migration of e-YSL beyond the blastoderm margin (white stippled line; upward arrows in **O**-**P**) after blue light treatment. EVL: enveloping layer; dc: deep cells.

Time Span of Plinabulin-induced Apoptosis in Zebrafish Embryos

Consequently, we opted to delve more precisely into the temporal progression of plinabulin-induced apoptosis, aiming to decipher the course of irreversible degeneration of the treated embryos. For this investigation, we treated wild-type embryos with 1 μM E-**1** at 4 hpf, followed immediately by subjecting one group of embryos to 490 nm irradiation for 60 minutes. The other set of embryos remained unexposed to irradiation (receiving 1 μM E-**1** or DMSO as a control). These embryos were allowed to develop at 28 °C until fixation at 6, 7.5, 9 and 10.5 hpf.

To identify apoptotic figures at each of these time points, we performed immunohistochemistry targeting activated caspase-3 (an apoptosis marker) in combination with DAPI nuclear staining. The results are illustrated in Figure 5. Furthermore, we
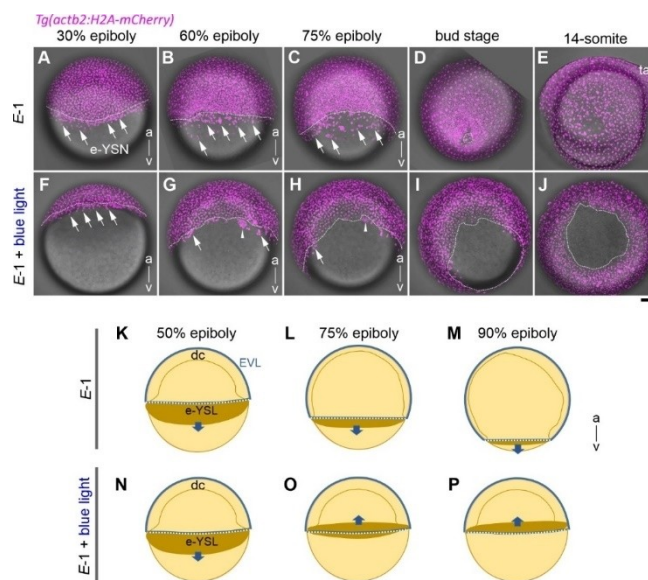
quantified the number of nuclei in embryos treated with E-**1** in darkness and under illumination, and compared these values with the untreated control. The outcome presented in Figure 5 illustrates that treatment with illuminated E-**1** significantly reduces the nucleus count and elevates the count of apoptotic figures.

Photoreversibility of Developmental Arrest with Plinabulin

The observed hours-range time difference between the reversible mitotic arrest and irreversible apoptosis caused by the more toxic Z-**1** isomer allowed us to demonstrate photoreversible developmental arrest of zebrafish embryos. For that, we have used the fact that different wavelengths of light cause photoequilibration of plinabulin to various ratios of photoisomers. In this particular case, cyan and UV light have an opposite effect. Starting from purified E-**1**, irradiation with cyan

ChemBioChem

Research Article
doi.org/10.1002/cbic.202400143

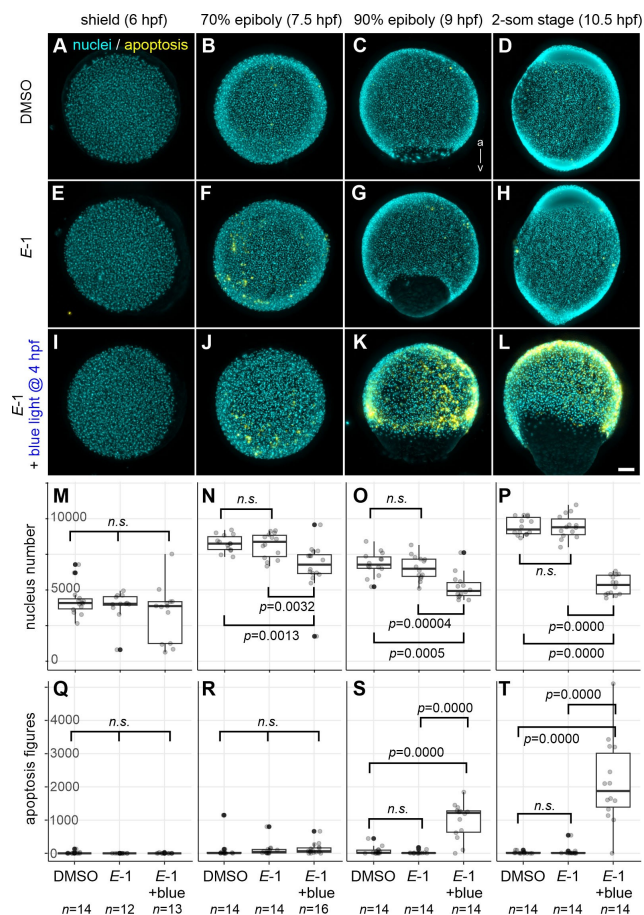Chemistry
Europe
European Chemical
Societies Publishing

Figure 5. Cyan Light-Induced Mitotic Arrest Followed by Apoptosis in *E*-1 Treated Embryos. Zebrafish embryos at 4 hpf were transferred to E3 medium containing DMSO (**A–D**) or *E*-1 (**E–L**). A subset of *E*-1-treated embryos underwent cyan light (490 nm) exposure for 1 hour (**I–L**). All embryo groups were subsequently grown in darkness until either 6 hpf (shield stage; **A, E, I**), 7.5 hpf (70% epiboly; **B, F, J**), 9 hpf (90% epiboly; **C, G, K**) or 10.5 hpf (2-som stage; **D, H, L**) and fixed for the analysis of nuclei number (DAPI staining; cyan) and apoptotic figures (immunohistochemistry using anti-activated caspase-3 antibody; yellow). Embryos were oriented either for the animal pole view (**A–B, E–F, I–J**) or the lateral view with the animal pole up and dorsal right (**C–D, G–H, K–L**). (**M–P**) Number of nuclei per individual embryo. Note that the absolute values from different stages are not directly comparable because of the fact that only one-third of the embryo was captured in 3D volumetric imaging. (**Q–T**) Number of apoptotic figures per individual embryo. *n.s.*: not significant; Scale bar: 100 μm; $n > 12$.

Figure 6. Reversible Embryo Growth Arrest with *E*-1 and Two Light Frequencies. Embryos were treated with 0.2 μM of *E*-1 at 4 hpf and immediately exposed to cyan light (490 nm, **B–C, E–F**) for 60 minutes to produce mostly *Z*-1 or left non-irradiated as control (**A, D**). At 5.5 hpf, part of the embryos was exposed to 365 nm irradiation for 12 minutes to convert most of the *Z*-1 into its less toxic *E*-isomer (**C, F**). Then, all embryos were rinsed with E3 medium at 6.5 hpf, to remove plinabulin from the environment. Afterwards, one group of embryos was incubated until 12 hpf and subsequently fixed and their apoptotic cells were stained (immunohistochemistry using anti-activated caspase-3 antibody; white spots; **A–C**). The other group was incubated until 48 hpf to analyze their phenotype for long-term development after treatment (**D–F**). The group treated without inactivation (exposure to the more toxic *Z*-1 isomer for 2.5 hours) displays a pronounced number of apoptotic cells at 12 hpf and predominantly malformed embryos with improperly developed heads and tails at 48 hpf (**B, E**; red asterisks). Embryos inactivated using UV light (365 nm) at 5.5 hpf (1.5 hours exposure to *Z*-1) exhibit a low number of apoptotic cells at 12 hpf and correctly developed heads, tails, and regular internal structure at 48 hpf (**C, F**).

light (490 nm) for 1 hour generates c.a. 69% of the toxic isomer *Z*-1. Subsequent irradiation of the same mixture with UV light (365 nm) restores c.a. 65% of the less toxic isomer *E*-1 (**Table S1**). Importantly, we did not observe adverse effects of UV light illumination by itself on the apoptosis figures at 12 hpf (*p*-adjusted = 0.95) and later morphology at 48 hpf (*p*-adjusted = 0.78). With that, we were able to find conditions where the embryos have been disturbed in their development and then remediated – both processes performed solely with light at precisely defined time periods - before the irreversible apoptosis pathway was initiated, so that the embryos continued growth and properly developed their head and tail parts (Figure 6, **Table S3**).
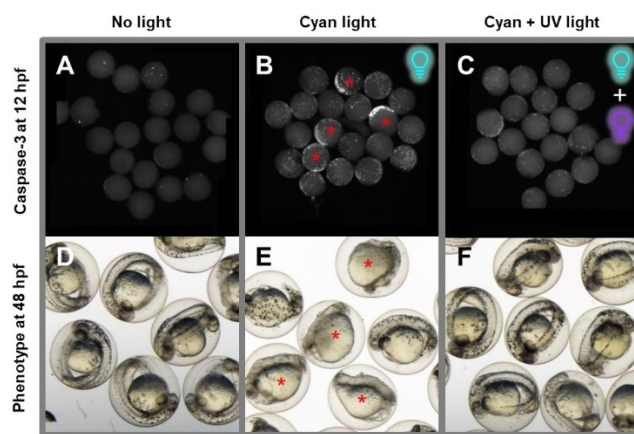
The initial LD$_{50}$ screening (Figure 2 and **Figure S5**) performed for the increasing concentrations of 0.1, 0.3, 1, 3, and 10 μM of **1** provided us with the good statistical toxicity approximation (concentration of respective compositions needed to kill 50% of the embryos). To perform the experiment where the effects of *Z*-1 are fully reversible, we needed to determine the concentration which efficiently causes the mitotic arrest, but does not elicit irreversible apoptosis that would lead to incorrect phenotype of the embryos (even if they are only "handicapped" and still remain alive). For that, we performed a series of screening experiments where we determined the "safe" concentration of the composition obtained upon irradiation of the less toxic *E*-1 with cyan light (490 nm). This value has been consistently determined to be the initial concentration of 0.2 μM of *E*-1 (see **Table S4**).

This composition has been incubated with zebrafish embryos and irradiated with cyan light (490 nm) to provide maximal conversion to the more toxic *Z*-1. Then, a part of the embryos was left exposed to that concentration, which caused apoptosis and ultimately death in most of the embryos after 48 hpf. The other part was additionally exposed to 365 nm UV illumination, which partially reverted the photoisomerization, and resulted in survival of most of the embryos after 48 hpf.

Staining for nuclei (DAPI) and immunostaining for tubulin, and caspase-3 (apoptosis marker) was once again conducted on embryos treated in the aforementioned manner after fixation at

ChemBioChem

Research Article
doi.org/10.1002/cbic.202400143

Chemistry Europe
European Chemical
Societies Publishing

7 hpf, as depicted in Figure 7. At a concentration of 0.2 μM *E*-**1**, the irradiation with 490 nm light at 4 hpf caused abnormal e-YSL with fewer nuclei and apoptosis (Figure 7B-**B'''** and **7 b**). However, embryos subsequently treated with UV light (365 nm) were successfully rescued (fewer apoptotic cells, and a normal e-YSL; Figure 7C–C''' and **7 c**). Apoptotic figures at 12 hpf (Figure 7D) were significantly increased with a group treated
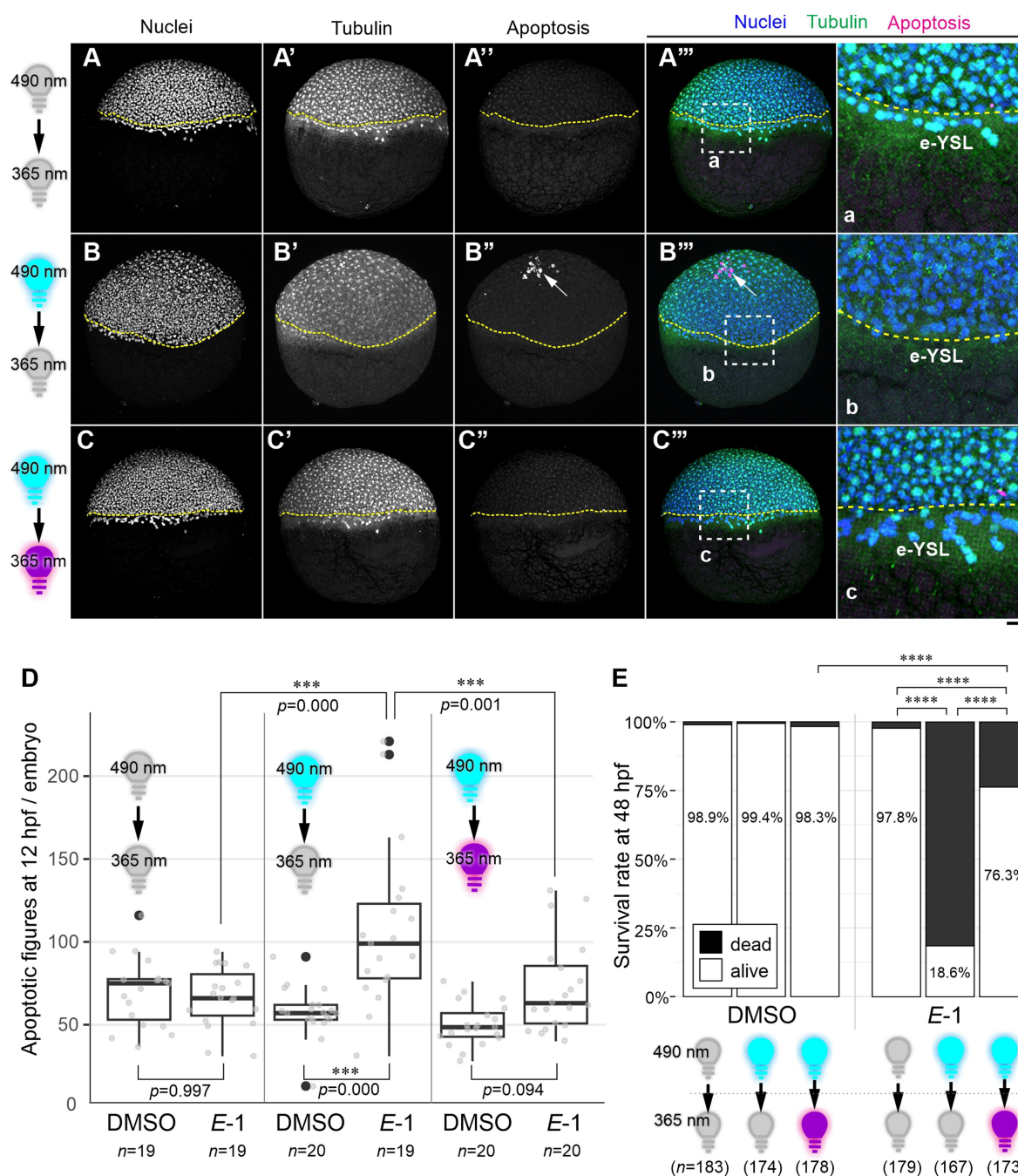

Figure 7. Light Controls the Apoptosis Induction Activity and Toxicity of 1. (**A–c**) Embryos at 4 hpf were incubated in **E3 medium containing** either DMSO or 0.2 μM *E*-**1** (all images shown here correspond to the incubation with *E*-**1**). Groups of embryos were either kept in the dark (**A-A'''**), illuminated only with 490 nm blue light at 4 hpf (**B–B'''**), or illuminated first with 490 nm at 4 hpf and subsequently at 5.5 hpf with 365 nm light (**C–C'''**) until they are fixed at 7 hpf for DAPI nuclear staining (**A–C**), immunohistochemistry for tubulin (**A'–C'**) and activated caspase-3 (apoptosis; **A''–C''**). Arrows indicate apoptotic figures. Yellow stippled lines demarcate the blastoderm margin. (**A'''–C'''**) Merged images for nuclei (blue, **A–C**), tubulin (green, **A'–C'**) and apoptosis channels (magenta, **A''–C''**). Magnified views of the regions in white stippled rectangles in **A'''–C'''** are shown in the panels **a–c**, respectively. e-YSL: external yolk syncytial layer. Note the reduced number of visible nuclei in the e-YSL after illumination with 490 nm, which was restored after second illumination of 365 nm light (**c**). Scale bar: 100 μm (**A–C'''**) or 25 μm (**a–c**). (**D**) Quantification of apoptotic figures at 12 hpf. *in situ* illumination of embryos with 490 nm light increased the number of observed apoptotic figures per embryo ($p = 0.000$), of which effect was partially rescued by subsequent 365 nm light illumination ($p = 0.094$ for DMSO vs *E*-**1** with 490 nm/365 nm illumination; $p = 0.001$ for *E*-**1** with 490 nm only vs 490 nm/365 nm illumination). Number of embryos for each group is shown at the bottom. (**E**) Survival rate analysis at 48 hpf. Number of embryos for each group is shown at the bottom. Illumination of 490 nm and 365 nm light were at 4 hpf and 5.5 hpf, respectively. Adjusted *p*-values of pairwise Fisher's test were calculated and denoted as ******** when the values are less than 0.0001.

ChemBioChem

Research Article
doi.org/10.1002/cbic.202400143

Chemistry
Europe
European Chemical
Societies Publishing

with 0.2 μM E-**1** upon 490 nm light illumination and partially rescued by subsequent UV light treatment.

To evaluate photomodulation of **1**'s activity in the context of embryonic development, we quantified the survival rate of embryos at 48 hpf after the same activation and inactivation procedures (Figure 7E). Illumination of 490 nm light on embryos treated with 0.2 μM E-**1** reduced the survival rate from 97.8% to 18.6% in comparison to non-illuminated group. In contrast, subsequent illumination of UV light restored the survival rate to 76.3%, demonstrating a substantial and significant rescue, albeit not a complete one.

Discussion

A variety of antimitotic agents can influence the process of cell division – as efficient anticancer drugs broadly used in clinics – as well as the development of whole experimental organisms upon efficient delivery. In order to control microtubule dynamics with higher precision, light-driven antimitotic agents have been introduced. One concept is irreversible photouncaging, that can be precisely performed in space and time,[33] however, this process is unidirectional and thus irreversible. An alternative concept is the use of photoswitchable antimitotic agents.[7,15] There, the light-induced inhibition of microtubule dynamics can be achieved reversibly – either by thermal deactivation,[16] diffusion from the irradiated area,[22] or upon treatment with another light frequency.[18] In the last case, microtubule dynamics inhibition can be reversed on demand. Here we have experimentally demonstrated the last of these possibilities for the first time at the scale of a whole organism.

In the first part, we have shown that we can interrupt the microtubule-dependent cell movement – epiboly – in the early development phase of a zebrafish embryo using a photo-switchable antimitotic agent plinabulin **1**. In presence of its more active Z-isomer (either generated in vitro, or in situ from the less active E-isomer using blue/cyan light), the embryos die within 12 hours after exposure, or – if Z-**1** is present in sublethal concentration – demonstrate severe malformations. We have analyzed this process at the cellular level using immunostaining as well as a zebrafish transgenic system with fluorescently labelled histones in cell nuclei. The observed picture is consistent with the inhibition of microtubule dynamics at the cellular and organismal level, namely the tubulin being abnormally distributed across the embryos, and the number of nuclei strongly reduced – the latter possibly resulting from intracellular mitotic arrest and thus reduced rate of cell proliferation.[29]

Our next observation was that above a certain concentration of Z-**1**, these cellular changes inevitably lead to embryo's death. However, below this value, the damage can be compensated to a certain degree, and living, albeit severely malformed, embryos are produced. This led us to the idea that the observed process has two distinctive phases – a reversible microtubule dynamic arrest, and an irreversible massive apoptosis causing death of the embryo. The latter occurs when the arrest lasts for too long time and affects too many cells throughout the embryo. Indeed, by immunostaining activated form of caspase-3 – an apoptosis reporter protein – we could identify the critical time span after treatment of embryos with Z-**1**, after which apoptosis becomes severe and embryo death becomes inevitable.

Based on this, we hypothesized that embryos treated with Z-**1** (or the less active E-**1** partially converted with blue/cyan light to the more toxic isomer) can be rescued from the irreversible apoptotic pathway and death if the more active Z-form is back-isomerized with UV-light, thereby restoring microtubule dynamics.

We have successfully tested this hypothesis by finding a concentration of plinabulin **1**, where we can reversibly switch between the toxic and non-toxic concentration of the Z-**1** form using two light wavelengths. At that concentration, the embryos treated with the less active E-**1** in darkness developed correctly at least until the 48 hpf stage. When our compound was activated with cyan light (490 nm) in the presence of embryos, this resulted in death or severe phenotypic malformations, as well as molecular effects visible in immunostaining. However, if the activation process was reverted early enough with UV light (365 nm), the embryos continued their development process and avoided detrimental malformations. The concentration of 0.2 μM E-**1** used in that experiment is lower than the previously determined LD_{50} value, as it allows to avoid also non-lethal phenotype alterations.

Conclusions

In conclusion, we have demonstrated that plinabulin **1** is the first photochromic inhibitor of microtubule dynamics that enables reversible photomodulation of the fate of a whole organism – either directly to death, or further development. Within that, we have validated that **1**: (a) can efficiently penetrate developing zebrafish embryos; (b) is operational in vivo as a molecular photoswitch with sufficient photo-conversions to reversibly elicit biological effects; and (c) retains the significant photomodulation of its biological activity at the organismal scale. With this set of unique properties, we are certain that **1** will successfully complement the available "molecular tools" for photomodulation of microtubule dynamics in biological systems.

In the future, we would like to demonstrate that **1** can be used in vivo with higher spatiotemporal resolution – not only to photomodulate the phenotype of a whole organism, but also to target selected tissues and groups of cells at a precisely defined moment of organismal development. We believe that **1** will become a great tool to dissect the roles of particular cells, e.g. by specifically targeting neurons during later zebrafish developmental stages using laser light.

Supporting Information

The authors have cited additional references within the Supporting Information.[34]

ChemBioChem

Research Article
doi.org/10.1002/cbic.202400143

Chemistry
Europe
European Chemical
Societies Publishing

Conflict of Interests

The authors declare no conflict of interest.

Data Availability Statement

The data that support the findings of this study are available in the supplementary material of this article.

[1] a) K. Deisseroth, G. Feng, A. K. Majewska, G. Miesenböck, A. Ting, M. J. Schnitzer, *J. Neurosci.* **2006**, *26*, 10380–10386; b) K. Deisseroth, *Nat. Neurosci.* **2015**, *18*, 1213–1225.

[2] A. M. J. Gomila, P. Gorostiza, in *Molecular Photoswitches*, **2022**, Wiley-VCH, pp. 811–842.

[3] Z. L. Pianowski, *Chem. Eur. J.* **2019**, *25*, 5128–5144.

[4] V. Koch, S. Bräse, in *Molecular Photoswitches*, **2022**, Wiley-VCH, pp. 39–64.

[5] a) K. Hüll, J. Morstein, D. Trauner, *Chem. Rev.* **2018**, *118*, 10710–10747; b) M. J. Fuchter, *J. Med. Chem.* **2020**, *63*, 11436–11447.

[6] M. Bispo, J. M. van Dijl, W. Szymanski, in *Molecular Photoswitches*, **2022**, Wiley-VCH, pp. 843–871.

[7] O. Thorn-Seshold, in *Molecular Photoswitches*, **2022**, Wiley-VCH, pp. 873–919.

[8] a) W. A. Velema, J. P. van der Berg, M. J. Hansen, W. Szymanski, A. J. M. Driessen, B. L. Feringa, *Nat. Chem.* **2013**, *5*, 924–928; b) M. Wegener, M. J. Hansen, A. J. M. Driessen, W. Szymanski, B. L. Feringa, *J. Am. Chem. Soc.* **2017**, *139*, 17979–17986.

[9] J. Ewert, L. Heintze, M. Jordà-Redondo, J.-S. von Glasenapp, G. Nonell, G. Bucher, C. Peifer, R. Herges, *J. Am. Chem. Soc.* **2022**, *144*, 15059–15071.

[10] O. Babii, S. Afonin, C. Diel, M. Huhn, J. Dommermuth, T. Schober, S. Koniev, A. Hrebonkin, A. Nesterov-Mueller, I. V. Komarov, A. S. Ulrich, *Angew. Chem. Int. Ed.* **2021**, *60*, 21789–21794.

[11] a) C. Matera, A. M. J. Gomila, N. Camarero, M. Libergoli, C. Soler, P. Gorostiza, *J. Am. Chem. Soc.* **2018**, *140*, 15764–15773; b) L. Josa-Culleré, A. Llebaria, *J. Med. Chem.* **2023**, *66*, 1909–1927.

[12] W. Szymanski, M. E. Ourailidou, W. A. Velema, F. J. Dekker, B. L. Feringa, *Chem. Eur. J.* **2015**, *21*, 16517–16524.

[13] a) M. Borowiak, F. Küllmer, F. Gegenfurtner, S. Peil, V. Nasufovic, S. Zahler, O. Thorn-Seshold, D. Trauner, H.-D. Arndt, *J. Am. Chem. Soc.* **2020**, *142*, 9240–9249; b) F. Küllmer, N. A. Vepřek, M. Borowiak, V. Nasufović, S. Barutzki, O. Thorn-Seshold, H.-D. Arndt, D. Trauner, *Angew. Chem. Int. Ed.* **2022**, *61*, e202210220.

[14] A. Müller-Deku, J. C. M. Meiring, K. Loy, Y. Kraus, C. Heise, R. Bingham, K. I. Jansen, X. Qu, F. Bartolini, L. C. Kapitein, A. Akhmanova, J. Ahlfeld, D. Trauner, O. Thorn-Seshold, *Nat. Commun.* **2020**, *11*, 4640.

[15] S. Kirchner, Z. Pianowski, *Int. J. Mol. Sci.* **2022** *23 (10)*, 5657.

[16] M. Borowiak, W. Nahaboo, M. Reynders, K. Nekolla, P. Jalinot, J. Hasserodt, M. Rehberg, M. Delattre, S. Zahler, A. Vollmar, D. Trauner, O. Thorn-Seshold, *Cell* **2015**, *162*, 403–411.

[17] a) A. Sailer, J. C. M. Meiring, C. Heise, L. N. Pettersson, A. Akhmanova, J. Thorn-Seshold, O. Thorn-Seshold, *Angew. Chem. Int. Ed.* **2021**, *60*, 23695–23704; b) L. Gao, J. C. M. Meiring, Y. Kraus, M. Wranik, T. Weinert, S. D. Pritzl, R. Bingham, E. Ntouliou, K. I. Jansen, N. Olieric, J. Standfuss, L. C. Kapitein, T. Lohmüller, J. Ahlfeld, A. Akhmanova, M. O. Steinmetz, O. Thorn-Seshold, *Cell Chem. Biol.* **2021**, *28*, 228–241.e226; c) A. Sailer, F. Ermer, Y. Kraus, R. Bingham, F. H. Lutter, J. Ahlfeld, O. Thorn-Seshold, *Beilstein J. Org. Chem.* **2020**, *16*, 125–134.

[18] S. Kirchner, A.-L. Leistner, P. Gödtel, A. Seliwjorstow, S. Weber, J. Karcher, M. Nieger, Z. Pianowski, *Nat. Commun.* **2022**, *13*, 6066.

[19] P. Godtel, J. Starrett, Z. L. Pianowski, *Chem. Eur. J.* **2023**, *29*, e202204009.

[20] A. Singh, T. Saha, I. Begemann, A. Ricker, H. Nüsse, O. Thorn-Seshold, J. Klingauf, M. Galic, M. Matis, *Nat. Cell Biol.* **2018**, *20*, 1126–1133.

[21] J. Zenker, M. D. White, R. M. Templin, R. G. Parton, O. Thorn-Seshold, S. Bissiere, N. Plachta, *Science* **2017**, *357*, 925–928.

[22] L. Gao, J. C. M. Meiring, A. Varady, I. E. Ruider, C. Heise, M. Wranik, C. D. Velasco, J. A. Taylor, B. Terni, T. Weinert, J. Standfuss, C. C. Cabernard, A. Llobet, M. O. Steinmetz, A. R. Bausch, M. Distel, J. Thorn-Seshold, A. Akhmanova, O. Thorn-Seshold, *J. Am. Chem. Soc.* **2022**, *144*, 5614–5628.

[23] J. Liu, M. Chen, X. Gao, X. Liu, J. Zhao, R. Pan, W. Zhong, Y. Xu, M. Wang, *Thorac. Cancer* **2023**, *14*, 773–778.

[24] A. V. Singh, M. Bandi, N. Raje, P. Richardson, M. A. Palladino, D. Chauhan, K. C. Anderson, *Blood* **2011**, *117*, 5692–5700.

[25] D. W. Blayney, R. Mohanlal, H. Adamchuk, D. V. Kirtbaya, M. Chen, L. Du, S. Ogenstad, G. Ginn, L. Huang, Q. Zhang, *JAMA Netw. Open* **2022**, *5*, e2145446-e2145446.

[26] M. Adhish, I. Manjubala, *Heliyon* **2023**, *9*.

[27] L. Yang, N. Y. Ho, R. Alshut, J. Legradi, C. Weiss, M. Reischl, R. Mikut, U. Liebel, F. Müller, U. Strähle, *Reprod. Toxicol.* **2009**, *28*, 245–253.

[28] C. B. Kimmel, W. W. Ballard, S. R. Kimmel, B. Ullmann, T. F. Schilling, *Dev. Dyn.* **1995**, *203*, 253–310.

[29] L. Solnica-Krezel, W. Driever, *Dev.* **1994**, *120*, 2443–2455.

[30] a) A. E. E. Bruce, *Dev. Dyn.* **2016**, *245*, 244–258; b) A. Hawdon, A. Aberkane, J. Zenker, *Dev.* **2021**, *148*.

[31] L. Carvalho, C.-P. Heisenberg, *Trends Cell Biol.* **2010**, *20*, 586–592.

[32] L. A. Rohde, C. P. Heisenberg, in *International Review of Cytology, Vol. 261*, Academic Press, **2007**, pp. 159–192.

[33] A. Döbber, A. F. Phoa, R. H. Abbassi, B. W. Stringer, B. W. Day, T. G. Johns, M. Abadleh, C. Peifer, L. Munoz, *ACS Med. Chem. Lett.* **2017**, *8*, 395–400.

[34] a) P. Aleström, L. D'Angelo, P. J. Midtlyng, D. F. Schorderet, S. Schulte-Merker, F. Sohm, S. Warner, *Lab. Anim.* **2020**, *54*, 213–224; b) U. Strähle, S. Scholz, R. Geisler, P. Greiner, H. Hollert, S. Rastegar, A. Schumacher, I. Selderslaghs, C. Weiss, H. Witters, T. Braunbeck, *Reprod. Toxicol.* **2012**, *33*, 128–132; c) M. Westerfield, *The zebrafish book. A guide for the laboratory use of zebrafish (Danio rerio)*. 4th ed., Univ. of Oregon Press, Eugene, **2007**; d) J. Schindelin, I. Arganda-Carreras, E. Frise, V. Kaynig, M. Longair, T. Pietzsch, S. Preibisch, C. Rueden, S. Saalfeld, B. Schmid, J.-Y. Tinevez, D. J. White, V. Hartenstein, K. Eliceiri, P. Tomancak, A. Cardona, *Nat. Methods* **2012**, *9*, 676–682; e) D. Ershov, M.-S. Phan, J. W. Pylvänäinen, S. U. Rigaud, L. Le Blanc, A. Charles-Orszag, J. R. W. Conway, R. F. Laine, N. H. Roy, D. Bonazzi, G. Duménil, G. Jacquemet, J.-Y. Tinevez, *Nat. Methods* **2022**, *19*, 829–832.